

A novel implementation of symmetric boundary condition in harmonic and transient analysis of electromagnetic wave propagation

Durgarao Kamireddy*, Sreekanth Karanam and Arup Nandy

Department of Mechanical Engineering, Indian Institute of Technology Guwahati, Guwahati 781039, India

ARTICLE INFO

Keywords:
 FEM
 Electromagnetics
 Symmetry boundary condition
 Harmonic analysis
 Transient analysis

ABSTRACT

While doing electromagnetic analysis using FEM, using symmetry, if exists will minimize the computational cost. Through the physical problem definition, it is possible to determine if symmetry exists about one plane for particular electromagnetic problems. The adoption of suitable symmetry boundary conditions can help to minimize the computing domain for these types of problems. But for electromagnetic analysis in potential formulation it is not very straight forward to implement the symmetric boundary condition. In the present work, a novel approach of implementation of symmetry boundary condition in potential formulation within nodal framework has been demonstrated. Also, it is implemented to various electromagnetic harmonic and transient problems. These problems include various domains such as conducting and dielectric sphere, cube with conducting walls and ellipsoid. A significant reduction in computational cost is achieved using the proposed method.

1. Introduction

In the field of computational electromagnetics, the importance of application of the finite element method (FEM) is universally well established. This field of research has a wide range of applications in antenna radiations, wave guide transmissions, cavity resonant problems, etc [45, 16]. In the conventional approach, while solving electromagnetic radiation and scattering problems using finite element method, the infinite region exterior to the scatterer/radiator must be truncated to reduce the size of the computational domain. Then, to absorb the outgoing wave radiation, some appropriate absorbing boundary condition (ABC) is imposed on the truncation surface [32]. This ABC is determined based on Sommerfeld radiation condition [8]. In [8, 25, 43, 46], certain second- and higher-order ABCs are given. In these works, authors have modeled the computational domain with both standard finite element method and Boundary Integral method (BI). Here, the interior domain is discretized with edge elements whereas, BI to the truncation surface. Even though this technique is more accurate than traditional ABCs, a key disadvantage is the problem of generation of densely populated matrix by BI elements which results in higher memory needs and calculation time. Other efficient method is the use of infinite element formulations. In this method, truncation surface which is surrounded by radiator/scatterer are meshed with conventional elements, whereas domain outside the surface is discretized with infinite elements. In [32], A Nandy et al. (2016) proposed an amplitude formulation for the exterior domain, harmonic, electromagnetic analysis for radiation and scattering problems in the framework of nodal finite element method. In this formulation, same element can be used in the complete domain as long as the origin is not part of the domain [32]. Various problems like scattering by conducting and dielectric sphere, conducting cylinder, conducting cube, conducting L shaped domain are solved and the results have been verified either with analytical solutions or with edge element results from HFSS [7]. At higher frequency Amplitude formulation is better than HFSS and conventional nodal formulation totally fails. The basic idea behind the use of the amplitude formulation is to a-priori separate the highly oscillatory e^{-ikr} section (r being the radial co-ordinate and k being the wavenumber) from the interpolation function so that the finite element requires to interpolate a more gentle function, which it does rather effectively even at higher frequencies. The Wilcox asymptotic expansion for electric field [30] from the radiator/scatter is used in this amplitude formulation. With nodal finite element, presence of spurious eigen values are well known limitations in literature. This can be partly eliminated using a penalty or regularization term [26, 34, 35, 38] and partly by using potential formulations [1]. But

*Corresponding author

 durga176103010@iitg.ac.in (D. Kamireddy); skaranam@iitg.ac.in (S. Karanam); arupn@iitg.ac.in (A. Nandy)
 ORCID(s):

these cannot predict singular eigen values for domains with sharp corners and edges. When the non-convex or inhomogeneous domain is involved, the situation becomes much worse. However, mixed finite formulation [18], predicted correct eigenvalues for both convex and non-convex domains except for the curved three-dimensional objects. To tackle this problem, the edge element employs the basis function associated with edge [4, 5, 6, 21, 22, 23, 19, 24, 20]. Edge elements enable tangential field continuity at element edges and properly represent the curl operator's null space. These elements enforce tangential continuity and normal discontinuity of the field variable across inter-element boundaries.

A wide range of numerical methods are available to solve Maxwell's electromagnetic wave equation in time domain ([45]). Among the two familiar methods such as Finite Difference Time Domain (FDTD) method and Time Domain FEM (TDFEM) method, former method gained popularity due to its simplicity in numerical integration. In [36], Yee introduced FDTD method to solve Maxwell's equations in isotropic media. Although this method gained popularity, TDFEM method reported in [9, 14, 27, 29, 31, 37, 44, 48] has major advantages in dealing with complex geometries. In TDFEM, two approaches are followed to solve for electromagnetic field variables. In first approach [14, 27, 44], second order electromagnetic wave equation is solved for either electric or magnetic fields. Then from post processing other fields are obtained. In the other approach [9, 31, 48], two coupled first order Maxwell's equations are solved for both field variables simultaneously. In [11, 14, 28, 37], another method, namely, Finite Element Boundary Integral (FEBI) method is applied to simulate the infinite domains by dividing into exterior and interior domains. These two domains are separated by an artificial boundary. Exterior domains are modeled with boundary integral method and interior domain with finite elements. In transient electromagnetic analysis, different time stepping strategies such as leapfrog strategy [39, 40, 41], central difference method [10, 14, 28] are used to discretize the time. Stability of the algorithm is an important factor in simulating electric and magnetic fields in transient analysis. In [33], authors have used the time stepping strategy in nodal element frame work for electromagnetic analysis, which is unconditionally stable from an energy perspective. It is well known, in numerical analysis, if symmetric boundary conditions can be implemented, it can reduce the computational cost. In the current research work, an attempt is made to introduce a novel method of application of the symmetric boundary condition for various harmonic and transient electromagnetic wave problems. We tried to solve the different harmonic analysis problems from [32] and as well as transient problems from [33] where we can implement symmetry boundary condition.

The remaining article is organized as follows: In section 1.1, a brief discussion about the identification of symmetry from the physics of the problem is presented. Then, in section 2, we have briefly presented the mathematical formulation along with finite element implementation for both harmonic and transient analysis. We have presented the implementation of symmetry boundary condition in potential formulation in section 3. Thereafter, in section 4 and section 5, we have solved various numerical examples having symmetry in harmonic and transient analysis respectively with the application of the proposed method. The achieved computational advantage in the proposed formulation has also been presented elaborately.

1.1. Identification of existence of symmetry from physics of problem

To apply the symmetry boundary conditions, geometry, external loading as well as boundary conditions should be symmetric about the plane. If the problem is symmetric then we can solve using half of the domain with proper implementation of symmetric boundary condition which results in significant reduction of the computational cost. Detailed numerical analysis has been done and electric fields are compared for both full and half domains along with benchmark values. In each and every case, results of both the domains are almost matching with analytical/benchmark values. Moreover, it is also observed that in all the cases, with adoption of the present method, electric fields are simulated efficiently with less percentage of unknowns than full domain. Thus, the proposed method can be computationally very efficient in electromagnetic analysis.

For example, consider an electromagnetic plane wave in the form $E = E_x e^{-ikz} \hat{i}$ impinges on a conducting sphere whose center is located at the origin as shown in Fig. 1. From the physical observation, we can observe the geometry of the sphere is symmetry about the origin. The incident wave have electric field components distributed along x -direction, and the wave is traveling along z -direction. So, the incident electromagnetic wave vector is symmetric about xz -plane. Then the resultant scattered electromagnetic field due to the presence of the conducting sphere will also be symmetric about xz -plane. Hence, we can solve considering half of the domain i.e. one hemisphere with the flat surface along xz -plane. On that symmetry plane we have to impose zero normal electric field as the symmetry boundary condition. So, on that plane it will be $E_y = 0$.

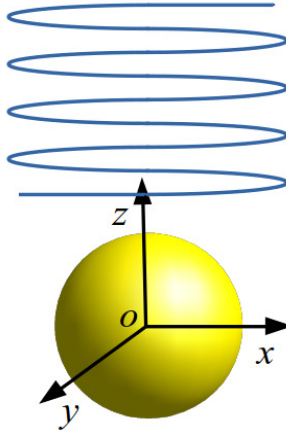


Figure 1: Plane electromagnetic wave incident on a conducting sphere.

2. Mathematical Formulation

We have Maxwell's electromagnetic wave equation in terms of electric field \mathbf{E} as stated in [13]

$$\frac{\epsilon_r}{c^2} \frac{\partial^2 \mathbf{E}}{\partial t^2} + \mu_0 \frac{\partial \mathbf{j}}{\partial t} + \nabla \times \left(\frac{1}{\mu_r} \nabla \times \mathbf{E} \right) = \mathbf{0}, \quad (1)$$

where $c = 1/\sqrt{\epsilon_0 \mu_0}$ is the speed of light and \mathbf{j} is the current density. Relative permittivity, ϵ_r and Relative permeability, μ_r are given as $\epsilon_r = \frac{\epsilon}{\epsilon_0}$ and $\mu_r = \frac{\mu}{\mu_0}$, where ϵ_0 and μ_0 are the permittivity and permeability for vacuum, and ϵ and μ are the electric permittivity and magnetic permeability of medium, respectively.

2.1. Harmonic analysis of Maxwell's equations

For harmonic excitation, Eq. 1 can be expressed as follows:

$$\nabla \times \left(\frac{1}{\mu} \nabla \times \mathbf{E} \right) - \frac{k^2}{\mu} \mathbf{E} = -i\omega \mathbf{j}, \quad (2)$$

where $i = \sqrt{-1}$. If ω is the excitation frequency then the wave number of vacuum is given as $k_0 = \omega/c$. And also, the wave number of the medium is related as $k = k_0 \sqrt{\mu_r \epsilon_r}$. For no charge condition, the electric field is subjected to following constraint

$$\nabla \cdot (\epsilon \mathbf{E}) = 0. \quad (3)$$

For perfectly conducting boundary (Γ_e) $\mathbf{E} \times \mathbf{n} = 0$ whereas for other part (Γ_h) $\mathbf{H} \times \mathbf{n}$ is prescribed. Assuming no surface currents exist at material discontinuity, both $\mathbf{E} \times \mathbf{n}$ and $\mathbf{H} \times \mathbf{n}$ must be continuous across the material interface [16]. In Potential formulation electric field \mathbf{E} is replaced as $\mathbf{A} + \nabla \psi$. So, the governing differential equation given by Eq. (2) and constraint equation Eq. (3) are modified as

$$\nabla \times \left(\frac{1}{\mu} \nabla \times \mathbf{A} \right) - \frac{k^2}{\mu} (\mathbf{A} + \nabla \psi) = -i\omega \mathbf{j}, \quad (4a)$$

$$\nabla \cdot (\epsilon \mathbf{A}) + \nabla \cdot (\epsilon \nabla \psi) = 0, \quad (4b)$$

The variational statements related to Eqs. (4a) and (4b) are given as equations 8a and 8b in [32] in which a regularization term relates to the coulomb gauge condition $\nabla \cdot \mathbf{A} = \text{constant}$, and the first-order absorbing boundary condition on truncated boundary (Γ_∞) is incorporated. Field variables \mathbf{A} , \mathbf{A}_δ , ψ , ψ_δ in equations 8a and 8b are discretized using the equation 9 in [32] as,

$$\mathbf{A} = \mathbf{N} \hat{\mathbf{A}}, \quad \mathbf{A}_\delta = \mathbf{N} \hat{\mathbf{A}}_\delta,$$

$$\psi = \mathbf{N}_\psi \hat{\psi},$$

$$\psi_\delta = \mathbf{N}_\psi \hat{\psi}_\delta.$$

The finite element equation has been obtained in [32] as

$$\begin{bmatrix} \mathbf{K}_{AA} & \mathbf{K}_{A\psi} \\ \mathbf{K}_{\psi A} & \mathbf{K}_{\psi\psi} \end{bmatrix} \begin{bmatrix} \hat{\mathbf{A}} \\ \hat{\psi} \end{bmatrix} = \begin{bmatrix} \mathbf{F}_A \\ \mathbf{F}_\psi \end{bmatrix}, \quad (5)$$

where the expressions for the terms \mathbf{K}_{AA} , $\mathbf{K}_{A\psi}$, $\mathbf{K}_{\psi A}$, $\mathbf{K}_{\psi\psi}$, \mathbf{F}_A , and \mathbf{F}_ψ are given by equation 10 in [32].

From the expansion theorem of Wilcox [47, 30], \mathbf{E} can be presented as

$$\mathbf{E} = \frac{e^{-ik|\mathbf{x}|}}{|\mathbf{x}|} \sum_{n=0}^{\infty} \frac{\mathbf{a}_n(\theta, \phi)}{|\mathbf{x}|^n}, \quad (6)$$

where $|\mathbf{x}|$ is the distance of a point from the origin, or, alternatively, the radial coordinate in the spherical coordinate system (r, θ, ϕ) . As in [2, 3, 17, 12], this expansion is used to separate out the rapidly-varying part $e^{-ik|\mathbf{x}|}/|\mathbf{x}|$. Therefore, the finite element shape functions only have to capture a gently-varying part [32]. From the amplitude formulation proposed in [32], (\mathbf{A}, ψ) and their variations $(\mathbf{A}_\delta, \psi_\delta)$ are expressed as equation 12, electric field \mathbf{E} and magnetic field \mathbf{H} are given as equation 13 from [32]. And also, the variational statements stated as equations 8a and 8b in [32] are modified to equations 15 and 16 in [32] respectively for the amplitude formulation. When origin is part of the domain, the entire domain is divided in two parts - the inner part is sphere containing the origin where conventional formulation is implemented and the outer part is hollow sphere where amplitude formulation is implemented. In order to have smooth transitions from the conventional towards the amplitude formulation, all the discretizations $(\bar{\mathbf{A}}, \bar{\mathbf{A}}_\delta, \bar{\psi}, \bar{\psi}_\delta)$ are multiplied with $r_1 e^{ikr_1}$ where r_1 is the radius of the interfacial spherical surface between inner and outer domain. For problems like radiation or scattering from conducting bodies, where the origin is not part of the computational domain, AMP elements are used. In the section 2.2.2 in [32] field variables and their variations are discretized as follows:

$$\begin{aligned} \bar{\mathbf{A}} &= \mathbf{N} \hat{\bar{\mathbf{A}}}, & \bar{\mathbf{A}}_\delta &= \mathbf{N} \hat{\bar{\mathbf{A}}}_\delta, \\ \bar{\psi} &= \mathbf{N}_\psi \hat{\bar{\psi}}, & \bar{\psi}_\delta &= \mathbf{N}_\psi \hat{\bar{\psi}}_\delta. \end{aligned}$$

In [32], resulting finite element equation is given as (see equation 17 in [32])

$$\begin{bmatrix} \mathbf{K}_{AA} & \mathbf{K}_{A\psi} \\ \mathbf{K}_{\psi A} & \mathbf{K}_{\psi\psi} \end{bmatrix} \begin{bmatrix} \hat{\bar{\mathbf{A}}} \\ \hat{\bar{\psi}} \end{bmatrix} = \begin{bmatrix} \mathbf{F}_A \\ \mathbf{F}_\psi \end{bmatrix}, \quad (7)$$

where from [32] we can see the expressions for the terms \mathbf{K}_{AA} , $\mathbf{K}_{A\psi}$, $\mathbf{K}_{\psi A}$, $\mathbf{K}_{\psi\psi}$, \mathbf{F}_A , and \mathbf{F}_ψ .

2.2. Transient analysis of Maxwell's equations

From the potential formulation proposed in [33], electric and magnetic fields are expressed in terms of $\mathbf{v} := \partial \mathbf{A} / \partial t$ and $\mathbf{w} := \partial(\nabla \psi) / \partial t$ as follows:

$$\mathbf{E} = -\mathbf{w} - \mathbf{v}, \quad (8)$$

$$\mathbf{H} = \frac{1}{\mu} \nabla \times \mathbf{A}. \quad (9)$$

In potential formulation, Eq. 1 and Eq. 3 are expressed as

$$\epsilon \left[\frac{\partial^2 \mathbf{A}}{\partial t^2} + \nabla \left(\frac{\partial^2 \psi}{\partial t^2} \right) \right] + \frac{\partial \mathbf{j}}{\partial t} + \nabla \times \left(\frac{1}{\mu} \nabla \times \mathbf{A} \right) = \mathbf{0}, \quad (10)$$

$$\nabla \cdot \left[\epsilon \left(\nabla \frac{\partial \psi}{\partial t} + \frac{\partial \mathbf{A}}{\partial t} \right) \right] = 0. \quad (11)$$

The variational statements are presented in equations 2.19 and 2.20 in [33] which are transformed in equations 2.23 and 2.24 after implementing suitable time strategies as expressed in equations 2.21 and 2.22 in [33]. Choice of time

stepping strategy is very crucial to conserve certain physical quantities with a view to make our numerical formulation unconditionally stable. As discussed in section 2.3 in [33], field variables and their variations are discretized as follows:

$$\begin{aligned} \mathbf{A} &= \mathbf{N} \hat{\mathbf{A}}, & \mathbf{A}_\delta &= \mathbf{N} \hat{\mathbf{A}}_\delta, \\ \psi &= \mathbf{N}_\psi \hat{\psi}, & \psi_\delta &= \mathbf{N}_\psi \hat{\psi}_\delta. \end{aligned}$$

We can derive various differential quantities of these variables as presented in [33] and the finite element equation can be written as

$$\begin{bmatrix} \mathbf{K}_{AA} & \mathbf{K}_{A\psi} \\ \mathbf{K}_{\psi A} & \mathbf{K}_{\psi\psi} \end{bmatrix} \begin{bmatrix} \hat{\mathbf{A}}_{n+1} \\ \hat{\Psi}_{n+1} \end{bmatrix} = \begin{bmatrix} \mathbf{f}_A \\ \mathbf{f}_\psi \end{bmatrix}. \quad (12)$$

Different submatrices and subvectors \mathbf{K}_{AA} , $\mathbf{K}_{A\psi}$, $\mathbf{K}_{\psi A}$, $\mathbf{K}_{\psi\psi}$, \mathbf{f}_A , and \mathbf{f}_ψ have been elaborately presented after equation 2.28 in [33].

3. Implementation of symmetric boundary condition using a thin patch

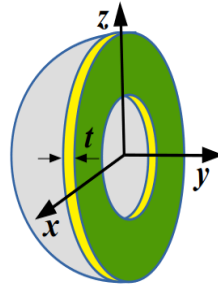


Figure 2: Sphere with a thin cylindrical patch of thickness, t .

In this section, we explain our novel method of implementation of symmetric boundary condition using a thin patch on the symmetry surfaces. Let us continue our discussion with the same example (Fig. 1) picked in section 1.1. In order to apply the symmetry boundary condition $E_n = 0$ on the symmetry boundary i.e., xz plane, a hollow cylindrical patch of very small thickness t is added as shown in Fig. 2. Here, the patch thickness t should be very small as compared to the other dimensions of the domain. The symmetric boundary condition ($\mathbf{E} \cdot \mathbf{n} = 0$) is applied in accordance with previously discussed potential formulation. On the outer green surface (see Fig. 2) of the cylindrical patch, the normal component of \mathbf{A} i.e., A_y are made to zero for all the nodes explicitly, to impose the condition ($\mathbf{A} \cdot \mathbf{n} = 0$). And also, to satisfy the condition $\nabla\psi \cdot \mathbf{n} = 0$, for all the nodes inside the volume of the cylindrical patch, $\psi = 0$ is applied explicitly. As the patch is very thin, it will result in $\nabla\psi \cdot \mathbf{n} = 0$ only on the green surface without disturbing the scattered field in the remaining domain. In the subsequent sections, we can see the efficacy of this method for various harmonic and transient problems.

4. Numerical examples with electromagnetic harmonic analysis

In this section, we apply the proposed method to implement symmetry boundary condition for both conventional potential formulation and Amplitude formulation for harmonic analysis with hexahedral 27 node brick (B27) and 18 node wedge (W18) elements. In our numerical analysis we have compared the simulation results of both full domain and half domains with proper modeling of symmetric boundary.

4.1. Scattering from a conducting sphere

The first example is taken from section 5.4 in [32]. Here, we want to solve for scattering electric fields from a conducting sphere. Let us consider a conducting sphere of radius a on which an electromagnetic plane wave $\mathbf{E}_{\text{inc}} = E_0 e^{-ikz} \mathbf{e}_x$ is incident. To implement FEM, our computational domain domain (air surrounding the conducting sphere) is hollow sphere which is truncated at radius R_∞ . On this truncated surface, we apply Sommerfeld absorbing boundary condition. Conducting boundary conditions is imposed on the inner spherical surface at radius a . Our interest is to find

the scattered electric field in the hollow spherical air domain having inner and outer radii of a and R_∞ respectively. From the discussion in section 1.1, we can treat the problem is symmetric about xz -plane. Therefore, we consider half of the hollow sphere as our computational domain. As discussed in the section 3 we apply symmetric boundary conditions explicitly on the symmetry face (xz). We discretize the truncated annular hemisphere with mesh size of $16 \times 12 \times 12$ B27 and W18 elements whereas for the thin cylindrical patch we used $16 \times 12 \times 1$ ($r \times \theta \times t$). In Table 1, mesh details along with total number of equations are presented for both full sphere and half sphere with thin patch.

Table 1

Mesh and equation details for half domain and full domain for scattering from a conducting sphere.

	Half sphere with thin patch	Full sphere [32]
Mesh size ($r \times \theta \times \phi$)	$16 \times 12 \times 12 +$ $16 \times 24 \times 1$	$16 \times 12 \times 24$
Number of equations	80125	106858

We have considered $k_0a = 1$, $k_0R_\infty = 5$ with $E_0 = 1$. At two different locations: (a) at near field ($k_0r = 1.15$) and (b) at far field ($k_0r = 4.75$), for $\theta = \frac{\pi}{4}$ real and imaginary scattered electric field components are plotted along ϕ in Fig. 3 and Fig. 4. During numerical analysis for half of the domain, we directly solve for $0 \leq \phi \leq \pi$, then we have $\mathbf{E}(\pi - \phi) = \mathbf{E}(\phi)$ because of symmetry of the problem for the remaining half domain. We can notice from both the plots (see Fig. 3 and Fig. 4) that the results from both full domain, half domain are closely matching with the analytical benchmark given as equation 33 in [32]. But the total numbers of equations are 25% less for the half domain (see Table 1) as compared to the full domain. As computational cost is directly co-related with the total no. of equations, hence proposed method is computationally very efficient.

4.2. Scattering from a conducting ellipsoid

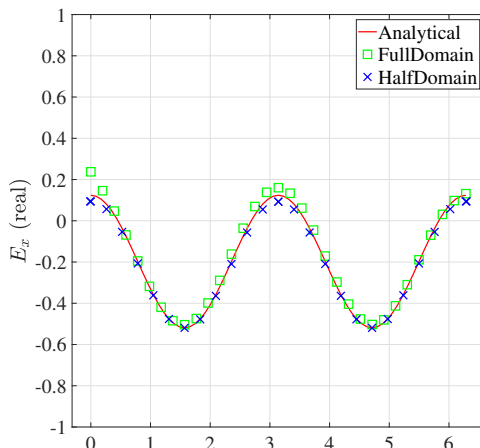
This example is chosen to show that the proposed implementation of symmetry boundary condition also works for non spherical geometry. A wave of the form $e^{-ik_0z}\mathbf{e}_x$ impinges on the ellipsoid having diameters $2a$, $2a$, and $2c$ along X , Y and Z axes, respectively. The domain is truncated at a spherical surface given by $k_0R_\infty = 24$. We present our results for $k_0a = 12$ and $c = a/4$. In this problem, the symmetry boundary condition $\mathbf{E} \cdot \mathbf{n} = \mathbf{0}$ is implemented as described in section 3. The half annular ellipsoidal domain is meshed with $12 \times 20 \times 8$ ($r \times \theta \times \phi$) B27 and W18 elements and an additional cylindrical patch has $12 \times 40 \times 1$ ($r \times \theta \times t$) B27 elements. Then we have to solve 73,949 equations. Table 2 summarizes the mesh details of half domain along with the full domain.

Table 2

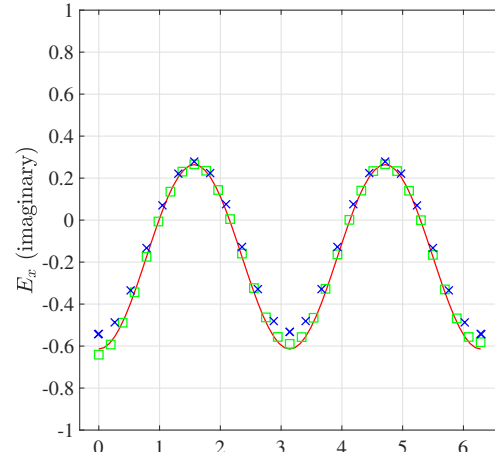
Mesh and equation details for half domain and full domain for scattering from a conducting ellipsoid.

Mesh size	half domain	full ellipsoid [32]
($r \times \theta \times \phi$)	$12 \times 20 \times 8 +$	$12 \times 20 \times 16$
($r \times \theta \times t$)	$12 \times 40 \times 1$	
Number of equations	73949	123018

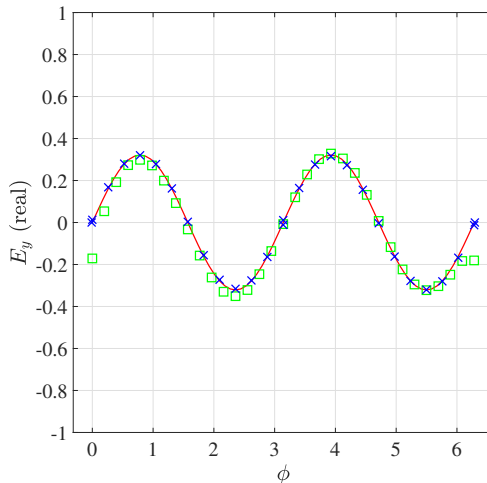
We have taken $E_0 = 1$, $k_0a = 12$, $k_0R_\infty = 24$. The scattered electric field components are compared in Fig. 5 along θ with $k_0r = 24$ and $\phi = \frac{\pi}{4}$. We have compared the results of half domain with symmetry (HDWS) in both conventional (Con) and amplitude formulation (OWF) with the converged HFSS [7] result obtained using a very fine mesh (1,49,530 unknowns i.e., unsuppressed degree of freedoms). In Fig. 5, we have also presented the respective full domain result for both Con and OWF formulations. In the current problem we directly solve for $0 \leq \phi \leq \pi$, because of symmetry of the problem we have $\mathbf{E}(2\pi - \phi) = \mathbf{E}(\phi)$ for the remaining half domain. We obtain equivalent accuracy with half domain (thin patch) using a system of equations having 40% less unknowns than that of full domain.



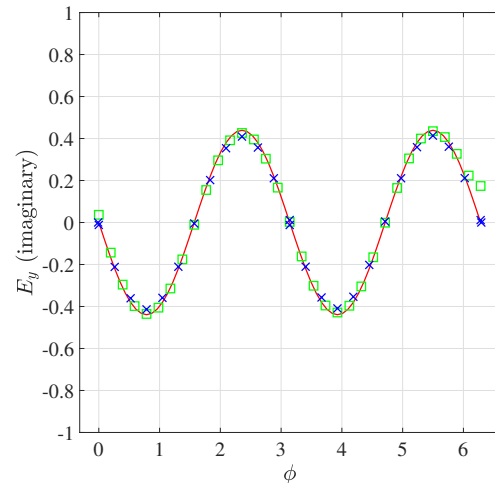
(a) E_x (real)



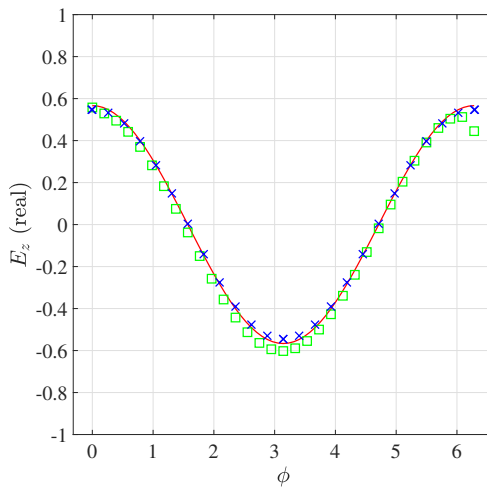
(b) E_x (imaginary)



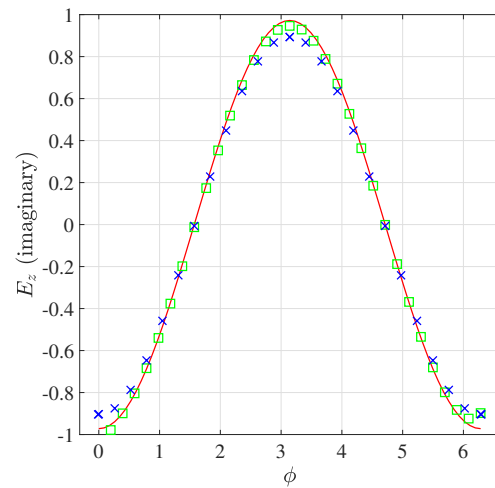
(c) E_y (real)



(d) E_y (imaginary)

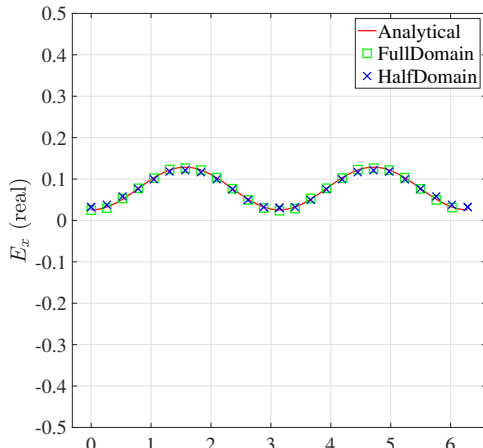


(e) E_z (real)

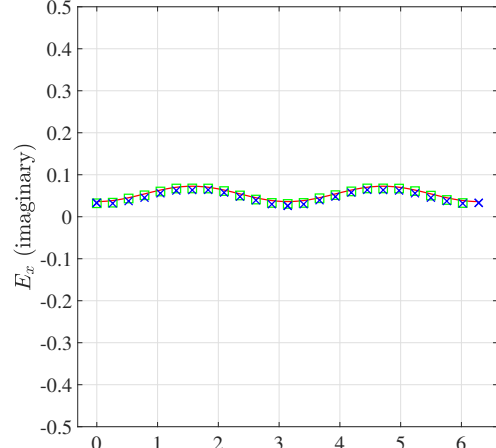


(f) E_z (imaginary)

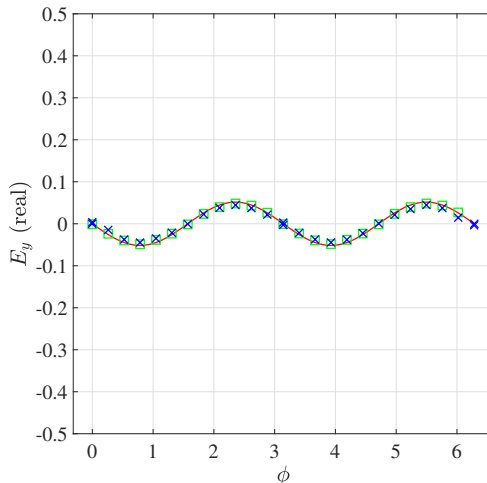
Figure 3: Plots showing the near field variation in the electric field for the scattering from a conducting sphere along ϕ for parameters $k_0r = 1.25$, $\theta = \pi/4$, $k_0a = 1$, $k_0R_\infty = 5$.



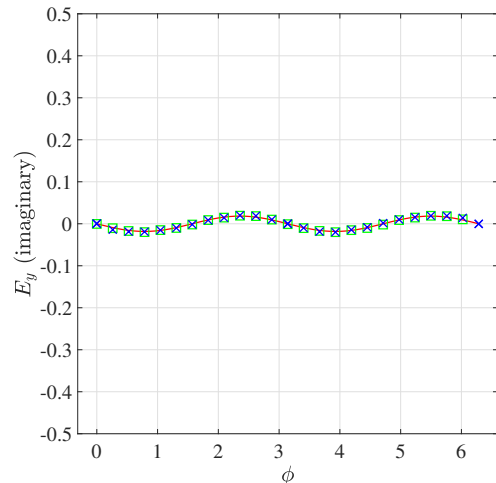
(a) E_x (real)



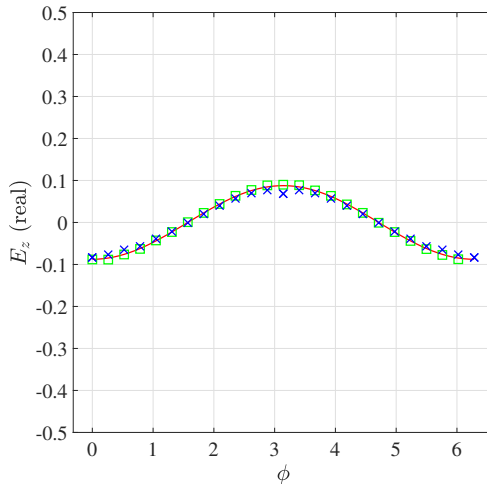
(b) E_x (imaginary)



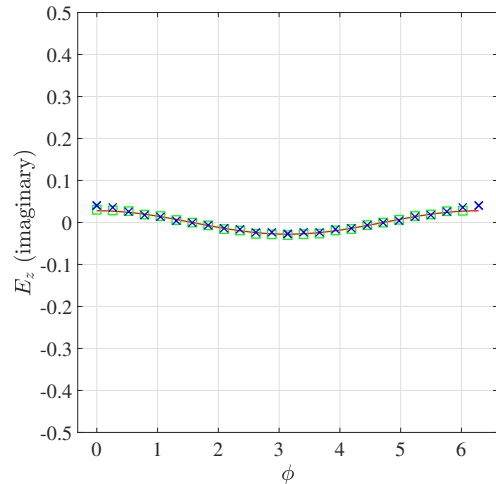
(c) E_y (real)



(d) E_y (imaginary)



(e) E_z (real)



(f) E_z (imaginary)

Figure 4: Plots showing the far field variation in the electric field for the scattering from a conducting sphere along ϕ for parameters $k_0r = 4.75$, $\theta = \pi/4$, $k_0a = 1$, $k_0R_\infty = 5$.

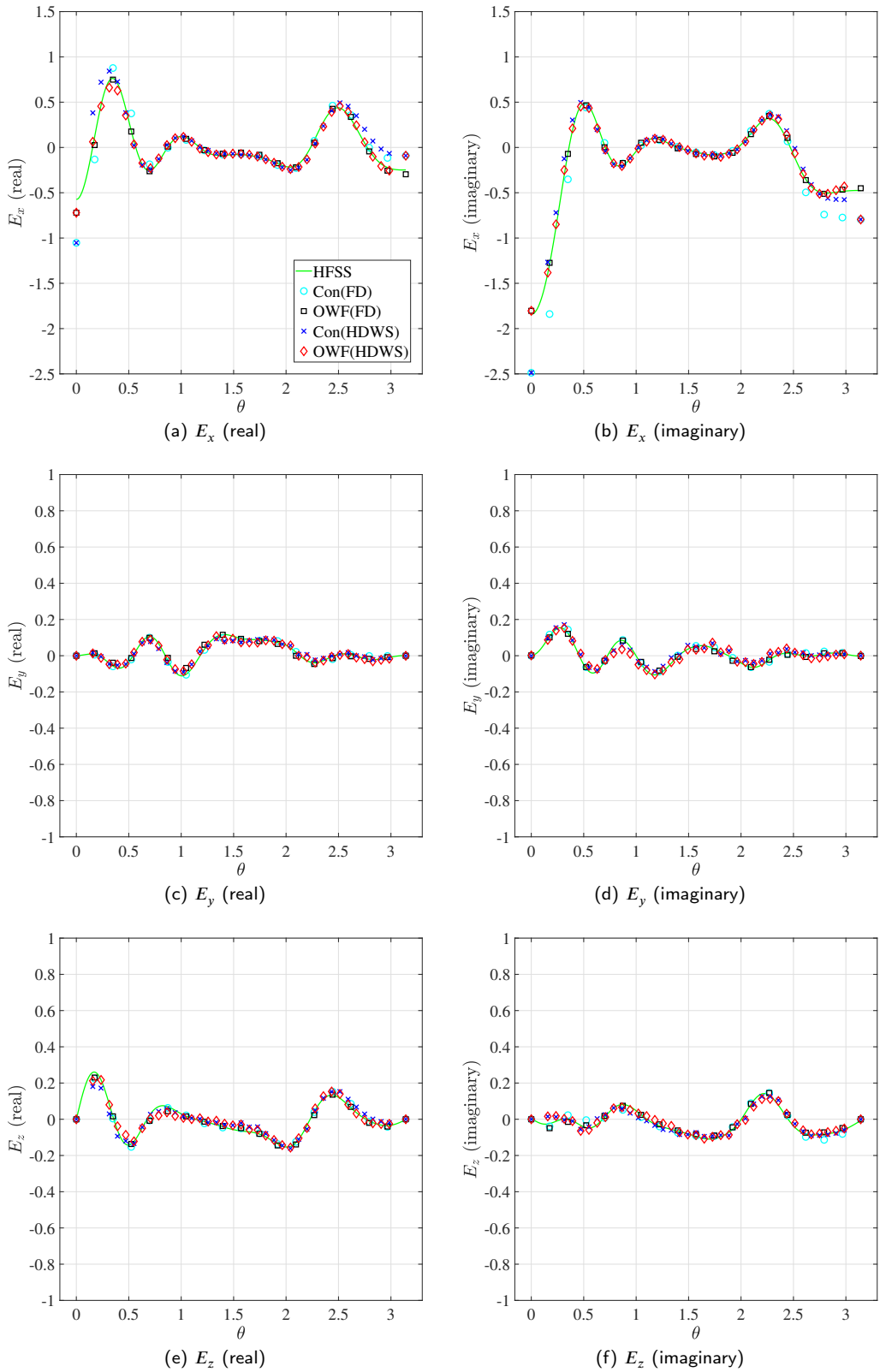


Figure 5: Electric field variation along θ for $k_0r = 24$, $\phi = \pi/4$, $k_0a = 12$, $k_0R_\infty = 24$ for the scattering from a conducting ellipsoid.

4.3. Scattering from a dielectric sphere

Consider an incident wave of the form $E_{\text{inc}} = E_0 e^{-ikz} \mathbf{e}_x$ impinges on a dielectric sphere. Let's assume the relative permeability and relative permittivity of the dielectric sphere and the surrounding medium be denoted by (μ_1, ϵ_1) and (μ_2, ϵ_2) , respectively. The analytical solution has been presented by Stratton [42]. In our numerical analysis, we assume the dielectric sphere to be in vacuum i.e., $\mu_2 = \epsilon_2 = 1$ and it has material properties $\mu_1 = 1$ and $\epsilon_1 = 1.5$. We choose $ka = 8$ and $kR_\infty = 24$ and the incident wave is of the form $e^{-ik_0 z} \mathbf{e}_x$. For both formulations i.e., conventional and amplitude formulation, 1000 B27 and W18 elements are used to mesh the half domain with symmetry plane, out of which 750 elements constitute the hemisphere and the remaining 250 B27 elements model the cylindrical patch of thickness $t = 0.01$. Mesh and equation details are given in Table 3. Since the origin is part of the domain, to mesh the dielectric sphere we use conventional nodal elements. Whereas, AMP elements are used to mesh the vacuum part of the domain.

Table 3

Mesh and equation details for half domain and full domain for scattering by dielectric sphere.

	half domain	full domain [32]
Mesh size	750(hemispherical domain) + 250(patch)	1500
Number of elements	1000	1500
Number of equations	28496	44692

Fig. 6 shows the results for the scattered electric field E_x inside the dielectric sphere at $k_0 r = 6.4$, at a point just outside the dielectric sphere ($k_0 r = 9.6$), and at a point in the far-field ($k_0 r = 16$) respectively. In all the plots, we have compared the results of both full domain (FD) and half domain with symmetry (HDWS) with analytical benchmark results as given by equation 34 in [32]. In Fig. 6, results from both conventional and OFWF formulations have been presented. In order to obtain same level of accuracy, for HDWS we have to solve around 36% less no. of equations as compared to the full domain which clearly depict the computational efficacy of the proposed method.

5. Numerical examples with electromagnetic transient analysis

In this section we apply the novel implementation of the symmetry boundary condition for various electromagnetic transient problems from [33] to analyze the efficacy of the proposed method in time domain. These problems includes radiation inside a cube with conducting faces, scattering from a conducting and dielectric sphere. Again, we choose B27 and W18 elements to discretize the computational domains and we take $c = 3 \times 10^8 / \sqrt{\epsilon_r \mu_r}$ m/s.

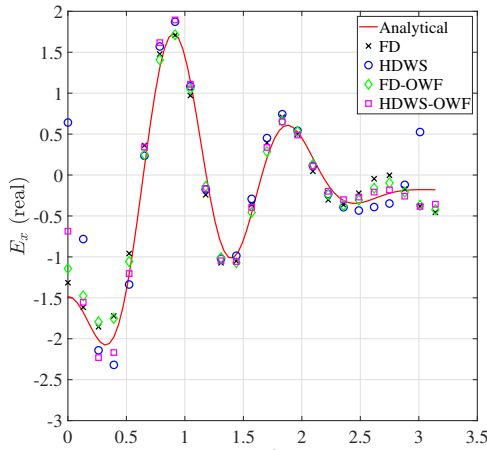
5.1. Electromagnetic radiation inside a cube with conducting walls

A cube of dimension $\pi \times \pi \times \pi$ with conducting walls is excited with \mathbf{j} and with initial \mathbf{A} values given as equation 3.2 in [33]. We have taken $\omega = 3 \times 10^8$ m/s, and simulated upto 4×10^{-8} sec with a time step of $t_\Delta = 1 \times 10^{-9}$ sec.

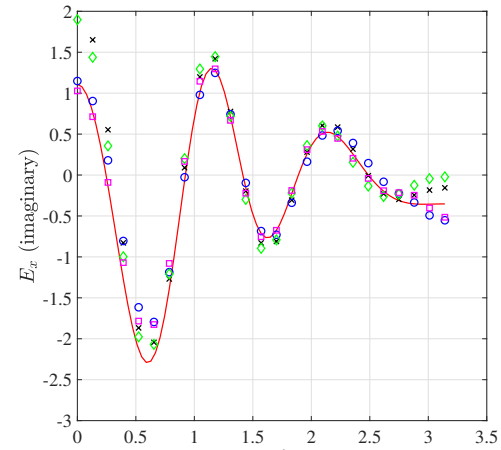
Table 4

Mesh and equation details for half domain and full domain of the cube.

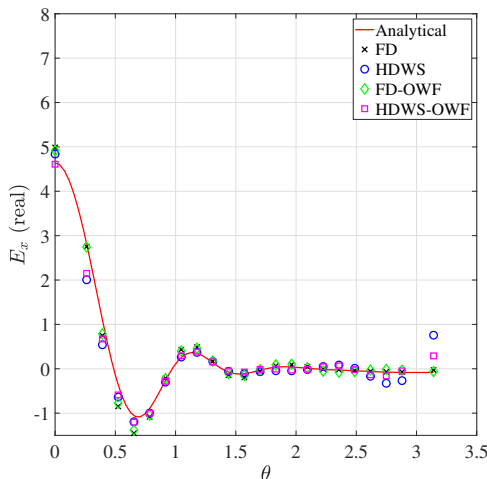
	half domain	cubical domain [33]
Mesh size ($x \times y \times z$)	$2 \times 4 \times 2$ (cuboid) + ($1 \times 4 \times 2$) + ($2 \times 4 \times 1$) + ($1 \times 4 \times 1$) (patches)	$8 \times 8 \times 8$
Number of elements	36	64
Number of equations	890	1666



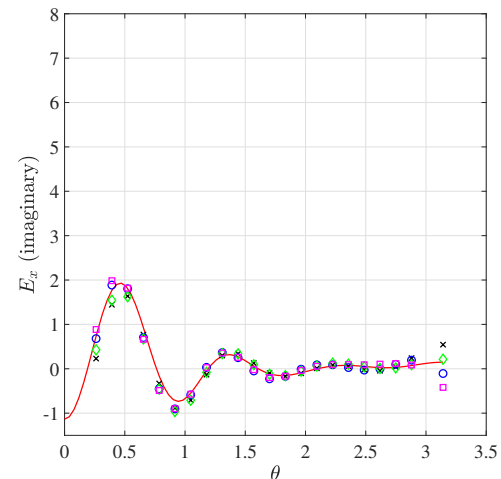
(a) $k_0r = 6.4, \phi = \pi/6$ (real)



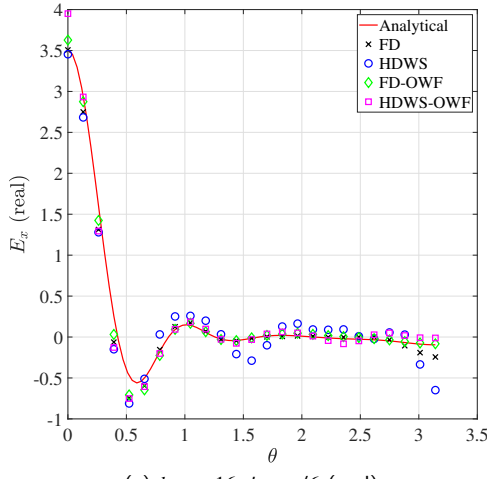
(b) $k_0r = 6.4, \phi = \pi/6$ (imaginary)



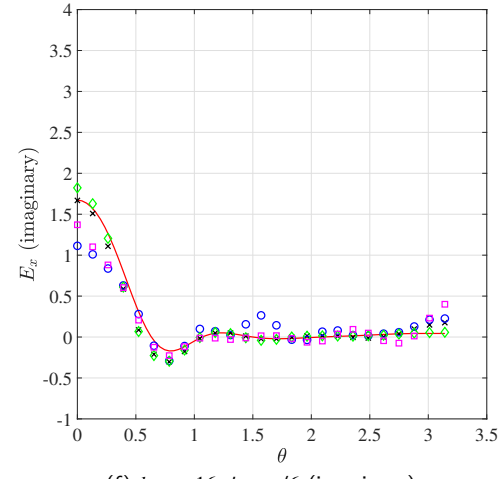
(c) $k_0r = 9.6, \phi = \pi/4$ (real)



(d) $k_0r = 9.6, \phi = \pi/4$ (imaginary)



(e) $k_0r = 16, \phi = \pi/6$ (real)



(f) $k_0r = 16, \phi = \pi/6$ (imaginary)

Figure 6: Variation of scattered electric field E_x along θ at different locations for the scattering from dielectric sphere problem.

To implement the symmetric boundary conditions, we truncated the cube from $\pi \times \pi \times \pi$ to cuboid with $\frac{\pi}{2} \times \pi \times \frac{\pi}{2}$. On the symmetry faces i.e., on xy and yz -planes, we have applied $\mathbf{E} \cdot \mathbf{n} = \mathbf{0}$ explicitly as explained in section 3, and on the remaining faces of the cuboid, conducting boundary conditions $\mathbf{E} \times \mathbf{n} = \mathbf{0}$ are applied. For transient analysis, 36 B27 elements are used to mesh cuboid and the thin patches, whereas full domain is meshed with 64 elements. Table 4 summarizes the numerical analysis details for both the domains. At a location with coordinates $(x, y, z) = (1.1780, 0, 0.3926, 0.7853)$, E_x , E_y , and E_z field components obtained for both full and half domains with symmetry are plotted in Fig. 7 and compared with analytical solutions given as equation 3.1 in [33]. Again, it is evident, by adopting the symmetric boundary conditions, 890 equations are sufficient for the perfect match with analytical benchmark as compared to 1666 unknowns for the full domain.

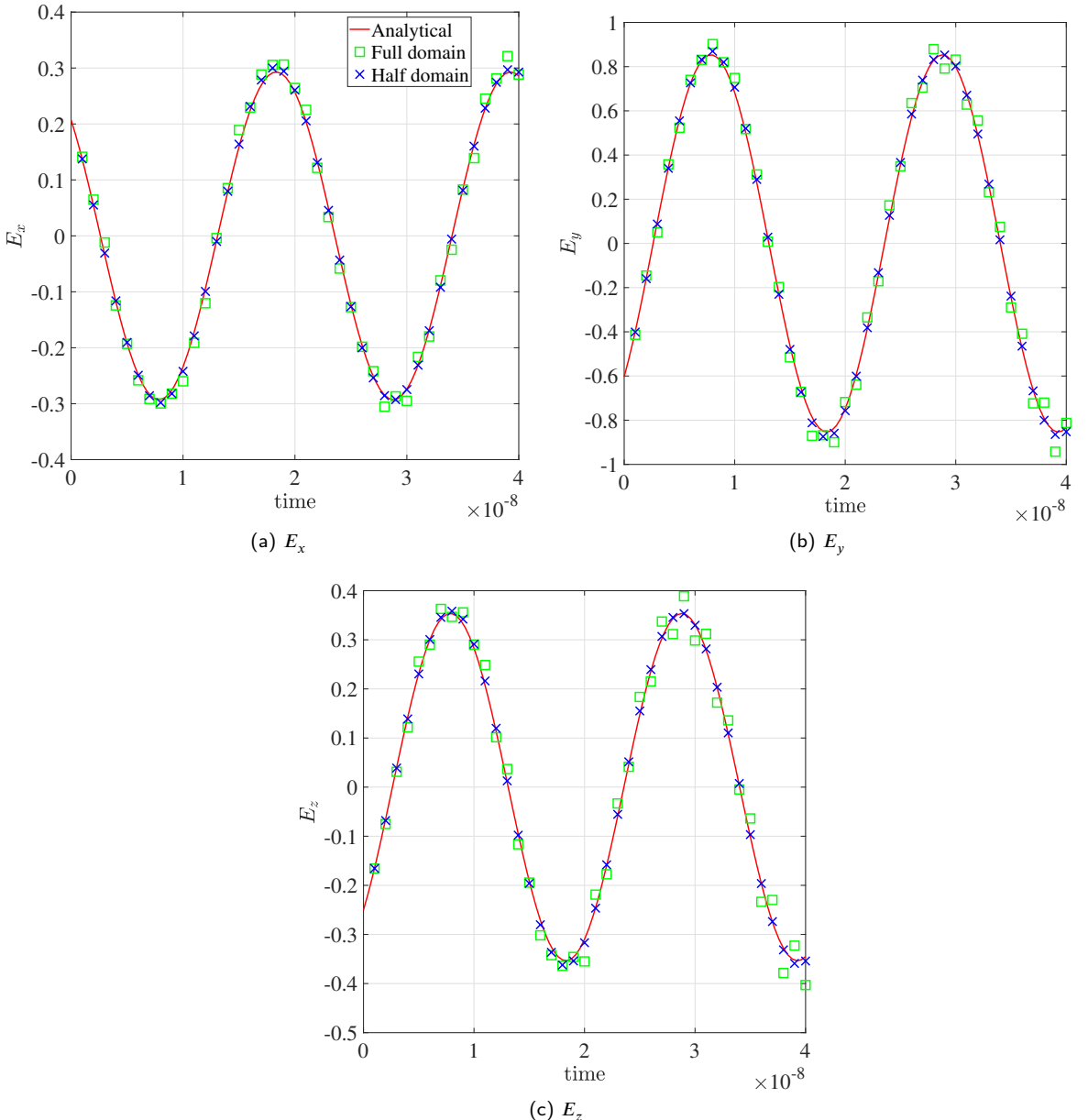


Figure 7: Variation of the electric fields at $(x, y, z) = (1.1780, 0, 0.3926, 0.7853)$ with respect to time for the cube with conducting walls.

5.2. Electromagnetic scattering from a conducting sphere

Table 5

Mesh and equation details for half domain and full domain of conducting sphere.

Mesh size	half domain	full sphere [33]
$(r \times \theta \times \phi)$	$8 \times 8 \times 5 +$	$8 \times 8 \times 10$
$(r \times \theta \times t)$	$8 \times 16 \times 1$	
Number of elements	448	640
Number of equations	11169	14946

To know the performance of the proposed method on curved objects, we consider the present example where we simulate the transient scattering electric fields from a conducting sphere. An incident wave given as equation 3.5 in [33] impinges on a conducting sphere, other problem parameters are followed same as section 3.6 in [33]. Computational full domain which is truncated at a radius $R_\infty = 3.8$ m is meshed with 640 B27 and W18 elements which results in 14,946 equations in [33]. In the current symmetry boundary condition implementation, the half domain with cylindrical patch is meshed with 448 B27 and W18 elements resulting in 11,169 equations (Table 5). Boundary conditions such as $\mathbf{E} \cdot \mathbf{n} = \mathbf{0}$ is implemented on the surface of the thin patch as described in section 3 and $\mathbf{E} \times \mathbf{n} = \mathbf{0}$ is applied on the conducting surface. We have taken a time step of 5×10^{-10} sec in our simulation. From Fig. 8, it is evident, $\frac{\partial E_x}{\partial t}$ values at a point $(0.33, -1.03, -0.45)$ in full domain and half domain with symmetry are perfectly matching with the standard benchmarks in [14]. Around 25% less unknowns have to be solved using symmetry boundary condition which clearly represent the computational efficacy of the proposed method.

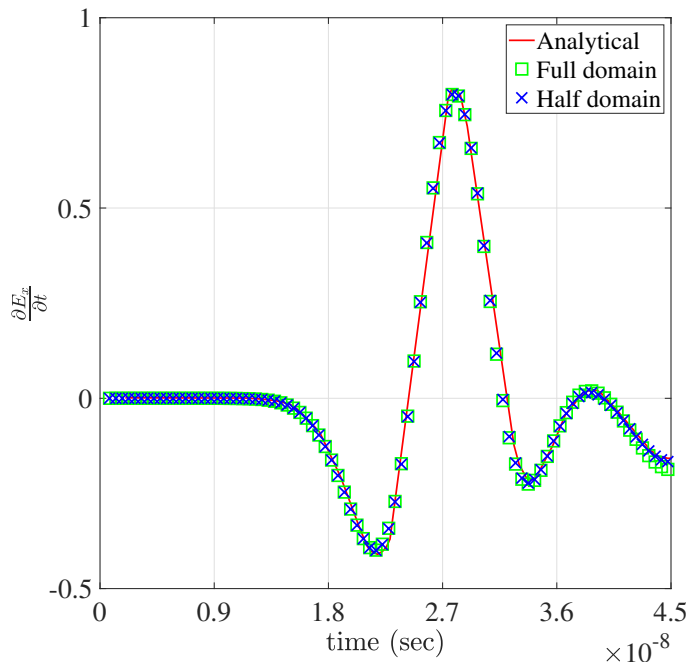


Figure 8: Time variation of the $\frac{\partial E_x}{\partial t}$ at $(x, y, z) = (0.33, -1.03, -0.45)$ for scattering from a conducting sphere.

5.3. Electromagnetic scattering from a dielectric sphere

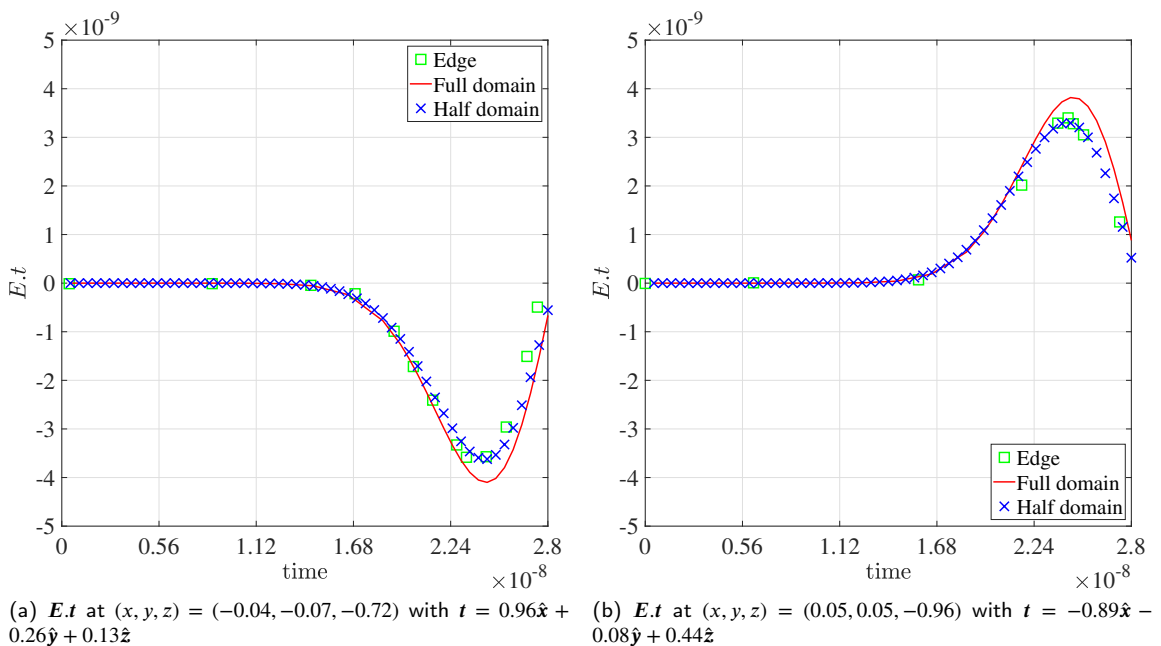
This example is chosen from section 3.7 in [33] to test the effectiveness of the proposed method in predicting scattering electric fields from a dielectric sphere. On a dielectric sphere of radius 0.5 m having $\mu_r = 1$ and $\epsilon_r = 6.0$,

Table 6

Mesh and equation details for half domain and full domain for scattering from a dielectric sphere.

	half domain	full domain
Mesh size	1536 (hemispherical domain) + 512 (patch)	3702
Number of elements	2048	3702
Number of equations	49076	70995

Neumann pulse wave as given in equation 3.5 in [33] is impinged. The computational domain which is truncated at radius $R_\infty = 2$ m is modeled with B27 and W18 elements. Table 6 gives the numerical analysis details for both full and half domains. Proper symmetric boundary condition is applied with thin cylindrical patch as described in section 3. With a time step of 0.5 ns simulations are performed. We have plotted $E \cdot t$ along time in Fig. 9 for full domain, half domain with symmetry and compared it with the benchmark edge element results in [15] at two locations: at (a) $(-0.04, -0.07, -0.72)$ with $t = 0.96\hat{x} + 0.26\hat{y} + 0.13\hat{z}$ and (b) $(0.05, 0.05, -0.96)$ with $t = -0.89\hat{x} - 0.08\hat{y} + 0.44\hat{z}$. Fig. 9 shows efficacy of our proposed method for transient scattering problem with dielectric body. Our proposed method predicts electric fields with only 49076 equations/unknowns which is 30% less as compared with the in full domain analysis.

**Figure 9:** Transient variation of the $E.t$ for scattering from a dielectric sphere.

6. Conclusions

In the present work, an attempt is made to implement symmetric boundary conditions to electromagnetic problems for both harmonic and transient analysis. In nodal framework, potential formulations are followed and it is not very straight forward to implement the symmetry boundary condition in that formulation. In the proposed method, a very thin patch is attached to the symmetry faces of the domain. Then, proper symmetric boundary conditions are applied

to the nodes of the thin patch explicitly. We have validated the proposed method solving a wide range of problems from radiation to scattering problems, from spherical to non-spherical domains, from harmonic to transient analysis. For all the problems we have validated our results against either analytical benchmark results or other benchmark from existing literatures. Furthermore, we have presented the computational efficacy of our proposed method as compared to existing full domain analysis for all the examples.

Acknowledgments

The authors gratefully acknowledge the support from SERB, DST under the project IMP/2019/000276, and VSSC, ISRO through MoU No.: ISRO:2020:MOU:NO: 480.

References

- [1] Arup Kumar Nandy, 2016. Robust Finite Element Strategies for Structures, Acoustics, Electromagnetics and Magneto-hydrodynamics. Ph.D. thesis. Indian Institute of Science Bangalore. Department of Mechanical Engineering, IISc, Bangalore, India. URL: <https://etd.iisc.ac.in/handle/2005/2913>.
- [2] Astley, R., 1983. Wave envelope and infinite elements for acoustical radiation. *International Journal for Numerical Methods in Fluids* 3, 507–526.
- [3] Astley, R.J., Eversman, W., 1983. Finite element formulations for acoustical radiation. *Journal of Sound and Vibration* 88, 47–64.
- [4] Boffi, D., Brezzi, F., Fortin, M., 2013. *Mixed Finite Element Methods and Applications*. Springer.
- [5] Boffi, D., Farina, M., Gastaldi, L., 2001a. On the approximation of maxwell's eigenproblem in general 2d domains. *Computers and Structures* 79, 1089–1096.
- [6] Boffi, D., Fernandes, P., Gastaldi, L., Perugia, I., 2001b. Computational models of electromagnetic resonators: Analysis of edge element approximation. *SIAM Journal on Numerical Analysis* 36, 1264–1290.
- [7] Cendes, Z., 2016. The development of hfss, in: 2016 USNC-URSI Radio Science Meeting, IEEE. pp. 39–40.
- [8] Chatterjee, A., Jin, J., Volakis, J.L., 1993. Edge-based finite elements and vector abcs applied to 3-d scattering. *IEEE transactions on antennas and propagation* 41, 221–226.
- [9] Chen, R.S., Lei, D., Ye, Z., Zhenbao, Yang, Y., 2009. An efficient algorithm for implementing the Crank-Nicolson scheme in the mixed finite-element time-domain method. *IEEE Transactions on Antennas and Propagation* 57, 3216–3222. doi:10.1109/TAP.2009.2028675.
- [10] D. Jiao, J. M. Jin, 2003. Three-dimensional orthogonal vector basis functions for time-domain finite element solution of vector wave equations. *IEEE Transactions on Antennas and Propagation* 51, 59–66. URL: <http://ieeexplore.ieee.org/document/1187416/>, doi:10.1109/TAP.2003.808524.
- [11] Faghihi, F., Heydari, H., 2008. A combination of time domain finite element-boundary integral with time domain physical optics for calculation of electromagnetic scattering of 3-D structures. *Progress in Electromagnetics Research* 79, 463–474. doi:10.2528/PIER07110206.
- [12] Geuzaine, C., Bedrossian, J., Antoine, X., 2008. An amplitude formulation to reduce the pollution error in the finite element solution of time-harmonic scattering problems. *IEEE Transactions on Magnetics* 44, 782–785.
- [13] Griffiths, D.J., 1999. *Introduction to Electrodynamics*. Second ed., Prentice Hall, New Jersey.
- [14] Jiao, D., Ergin, A.A., Shanker, B., Michielssen, E., Jins, J.M., 2002. A fast higher-order time-domain finite element-boundary integral method for 3-D electromagnetic scattering analysis. *IEEE Transactions on Antennas and Propagation* 50, 1192–1202. doi:10.1109/TAP.2002.801375.
- [15] Jiao, D., Jin, J.M., Michielssen, E., Riley, D.J., 2003. Time-domain finite-element simulation of three-dimensional scattering and radiation problems using perfectly matched layers. *IEEE transactions on antennas and propagation* 51, 296–305.
- [16] Jin, J.M., 2015. *The finite element method in electromagnetics*. John Wiley & Sons.
- [17] Jog, C.S., 2012. An outward-wave-favoring finite element based strategy for exterior acoustic problems. *International Journal of Acoustics and Vibration* 18, 27–38.
- [18] Jog, C.S., Nandy, A., 2014. Mixed finite elements for electromagnetic analysis. *Computers & Mathematics with Applications* 68, 887–902.
- [19] Kamireddy, D., Chavan, S.M., Nandy, A., 2022a. Comparative performance of novel nodal-to-edge finite elements over conventional nodal element for electromagnetic analysis. *Journal of Electromagnetic Waves and Applications* 0, 1–29. URL: <https://doi.org/10.1080/09205071.2022.2117102>, doi:10.1080/09205071.2022.2117102.
- [20] Kamireddy, D., Madhukar Chavan, S., Nandy, A., 2022b. Electromagnetic eigen analysis: Performance comparison of four node and four edge quadrilateral elements with the effect of distortion. *Materials Today: Proceedings* 66, 1968–1972. URL: <https://www.sciencedirect.com/science/article/pii/S2214785322037506>, doi:<https://doi.org/10.1016/j.matpr.2022.05.434>. 2022 International Conference on Recent Advances in Engineering Materials.
- [21] Kamireddy, D., Nandy, A., 2020. Combination of Triangular and Quadrilateral Edge Element for the Eigenvalue Analysis of Electromagnetic Wave Propagation. *European Journal of Molecular & Clinical Medicine* 7, 1656–1663.
- [22] Kamireddy, D., Nandy, A., 2021. Creating edge element from four node quadrilateral element. *IOP Conference Series: Materials Science and Engineering* 1080, 012015. URL: <https://doi.org/10.1088/1757-899x/1080/1/012015>, doi:10.1088/1757-899x/1080/1/012015.
- [23] Kamireddy, D., Nandy, A., 2022. A novel conversion technique from nodal to edge finite element data structure for electromagnetic analysis. *Computer Assisted Methods in Engineering and Science* 28, 291–319. doi:10.24423/cames.384. available online <https://cames.ippt.pan.pl/index.php/cames/article/view/384>.

[24] Kamireddy, D., Nandy, A., 2023. Conversion algorithm from nodal to edge finite element data structure for higher order elements, in: Manik, G., Kalia, S., Verma, O.P., Sharma, T.K. (Eds.), *Recent Advances in Mechanical Engineering*, Springer Nature Singapore, Singapore. pp. 619–629.

[25] Kanellopoulos, V., Webb, J., 1991. A numerical study of vector absorbing boundary conditions for the finite-element solution of maxwell's equations. *IEEE microwave and guided wave letters* 1, 325–327.

[26] Koshiba, M., Hayata, K., Suzuki, M., 1991. Finite element formulation in terms of the electric field vector for electromagnetic waveguide problems. *IEEE Transactions on Microwave Theory and Techniques* 33, 900–905.

[27] Lee, J., Lee, R., Cangellaris, A., 2002. Time-domain finite-element methods. *Antennas and Propagation, IEEE Transactions on* 45, 430–442. URL: [papers://501af03f-617f-4c97-a0b6-1b5282525b48/Paper/p1965](https://ieeexplore.ieee.org/stamp/stamp.jsp?tp=&arnumber=1021111).

[28] Liu, J., Jin, J.M., 2001. A novel hybridization of higher order finite element and boundary integral methods for electromagnetic scattering and radiation problems. *IEEE Transactions on Antennas and Propagation* 49, 1794–1806. doi:10.1109/8.982462.

[29] Member, J.F.L., 1994. WETD-A Finite Element Time-Domain Approach for Solving Maxwell's Equations. *IEEE Micrwave and Guided Wave Letters* 4, 11–13.

[30] Mittra, R., Ramahi, O., Khebir, A., Gordon, R., Kouki, A., 1989. A review of absorbing boundary conditions for two and three-dimensional electromagnetic scattering problems. *IEEE Transactions on Magnetics* 25, 3034–3039.

[31] Movahhedi, M., Abdipour, A., Nentchev, A., Dehghan, M., Selberherr, S., 2007. Alternating-direction implicit formulation of the finite-element time-domain method. *IEEE Transactions on Microwave Theory and Techniques* 55, 1322–1331. doi:10.1109/TMTT.2007.897777.

[32] Nandy, A., Jog, C.S., 2016. An amplitude finite element formulation for electromagnetic radiation and scattering. *Computers & Mathematics with Applications* 71, 1364–1391.

[33] Nandy, A., Jog, C.S., 2018. Conservation Properties of the Trapezoidal Rule for Linear Transient Electromagnetics. *Journal of Advances in Mathematics and Computer Science* 26, 1–26. URL: <http://www.sciencedomain.org/abstract/23334>, doi:10.9734/JAMCS/2018/39632.

[34] Otin, R., 2010. Regularized maxwell equations and nodal finite elements for electromagnetic field computations. *Electromagnetics* 30, 190–204.

[35] Paulsen, K.D., Lynch, D.R., 1991. Elimination of vector parasites in finite element maxwell solutions. *IEEE Transactions on Microwave Theory and Techniques* 39, 395–404.

[36] Pile, D., 2015. Numerical solution. *Nature Photonics* 9, 5–6. URL: <http://www.nature.com/articles/nphoton.2014.305>, doi:10.1038/nphoton.2014.305.

[37] Qiu, Z.J., Xu, J.D., Wei, G., Hou, X.Y., 2007. An improved time domain finite element-boundary integral scheme for electromagnetic scattering from 3-D objects. *Progress In Electromagnetics Research* 75, 119–135. URL: <http://www.jpier.org/PIER/pier.php?paper=07053106>, doi:10.2528/PIER07053106.

[38] Rahman, B.M.A., Davies, J.B., 1984. Penalty function improvement of waveguide solution by finite elements. *IEEE Transactions on Microwave Theory and Techniques* 32, 922–928.

[39] Rieben, R.N., Rodrigue, G.H., White, D.A., 2005. A high order mixed vector finite element method for solving the time dependent Maxwell equations on unstructured grids. *Journal of Computational Physics* 204, 490–519. doi:10.1016/j.jcp.2004.10.030.

[40] Rodrigue, G., White, D., 2001. A vector finite element time-domain method for solving maxwell's equations on unstructured hexahedral grids. *SIAM Journal on Scientific Computing* 23, 683–706. URL: <https://doi.org/10.1137/S1064827598343826>, doi:10.1137/S1064827598343826, arXiv:<https://doi.org/10.1137/S1064827598343826>.

[41] Sekine, T., Asai, H., 2011. Mixed finite element time domain method based on iterative leapfrog scheme for fast simulations of electromagnetic problems. *IEEE International Symposium on Electromagnetic Compatibility* , 596–601doi:10.1109/ISEMC.2011.6038381.

[42] Stratton, J.A., 2007. *Electromagnetic theory*. volume 33. John Wiley & Sons.

[43] Stupfel, B., 1997. Numerical implementation of second-and third-order conformal absorbing boundary conditions for the vector-wave equation. *IEEE Transactions on Antennas and Propagation* 45, 487–492.

[44] Tsai, H.P., Wang, Y., Itoh, T., 2002. An unconditionally stable extended (USE) finite-element time-domain solution of active nonlinear microwave circuits using perfectly matched layers. *IEEE Transactions on Microwave Theory and Techniques* 50, 2226–2232. doi:10.1109/TMTT.2002.803442.

[45] Volakis, J.L., Volakis, J.L., Chatterjee, A., Kempel, L.C., 1998. *Finite element method for electromagnetics*. Universities Press.

[46] Webb, J., Kanellopoulos, V., 1989. Absorbing boundary conditions for the finite element solution of the vector wave equation. *Microwave and Optical Technology Letters* 2, 370–372.

[47] Wilcox, C.H., 1956. An expansion theorem for electromagnetic fields. *Communications on Pure and Applied Mathematics* 9, 115–134.

[48] Wong, M.F., Picon, O., Hanna, V.F., 1995. Finite Element Method Based On Whitney Forms. *IEEE Transactions on Magnetics* 31, 4–7.